Estimating rockfall frequency in a mountain limestone cliff using terrestrial laser scanner

A Guerin, J-P Rossetti, D Hantz, M Jaboyedoff

Estimating rockfall frequency in a mountain limestone cliff using terrestrial laser scanner

A. Guerin[1], J-P. Rossetti[1], D. Hantz[1], M. Jaboyedoff[2]

[1]{ Univ. Grenoble Alpes, Univ. Savoie Mont Blanc, CNRS, IRD, Univ. Gustave Eiffel, ISTerre, 38000 Grenoble, France}

[2]{Centre de Recherche sur l'Environnement Terrestre, Université de Lausanne, Switzerland}

Correspondence to: D. Hantz (didier.hantz@univ-grenoble-alpes.fr)

This report was written in 2013

Abstract

Terrestrial laser scanner has been used to detect rockfalls which occurred in a high rock wall of the Subalpine Chains, from a survey station located up to 900 m from the cliff. Using a threshold of 0.1 m in term of distance variation, 344 rockfalls larger than 0.05 m^3 have been detected for a period of 1180 days, in a rock wall of width 750 m and height 200 m. The complementary cumulative distribution of the rockfall volume is well fitted by a power law, with an exponent b of 0.75 ± 0.04. In order to compare the rockfall frequencies in different geological contexts, a rockfall activity parameter has been considered, which is the number of rockfalls larger than a given volume, which occur per century and per hm^2. For the thinly bedded limestone making the cliff surveyed, the number of rockfalls larger than 1 m^3 is 0.85 rockfalls per year and per hm^2. It is two orders of magnitude higher than the number obtained for massive limestone cliffs of the Subalpine Chains in the Grenoble area.

1 Introduction

Estimating rockfall frequency is needed to characterize a diffuse rockfall hazard (Hungr, 1999; Picarelli et al., 2005; Fell et al., 2005; Hantz, 2011). Up to now this frequency is determined from historical inventories. The minimal volume detected in these inventories can be relatively small when the rock blocks fall on a road or railway from a cut slope, but it is larger when they

fall from a high rock cliff (Dussauge et al., 2002). In the last years, terrestrial laser scanner (TLS) has been used to detect rockfalls by comparing digital cliff models obtained from successive datasets.

On the east coast of the Great Britain, Rosser et al. (2005) detected 810 rockfalls greater than 10^{-3} m^3, occurred during 16 months in a coastal cliff of 300 m in width and 65 m in height. In the same area, Lim et al. (2010) detected 114,500 rockfalls occurred in a period of 20 months in 5 cliffs covering 16,000 m^2, the height of which ranging from 35 m to 70 m. The small distance from the survey station to the cliff face (maximum 70 m) allowed them to detect rockfalls as small as 1.25×10^{-4} m^3. These cliffs are formed from mudstone, shale, siltstone and sandstone. On the coast of Normandy (France), Dewez et al. (2013) detected 8500 rockfalls greater than 10^{-3} m^3, occurred in a period of 27 months in a chalk coastal cliff of 50 m in height and 750 m in width.

In Catalonia (Spain), Abellan et al. (2010 ; 2011) have monitored two continental cliffs from a distance of about 100 m. They considered a detection threshold of 10^{-3} m^3, according to Rosser et al. (2005). A number of 42 rockfalls were detected in a period of 10 months in a cliff of 25 m in height and 150 m in width, formed from sedimentary rocks (marl, sandstone, silt, clay), and 7 rockfalls were detected in a period of 22 months in a basaltic cliff of 35 m in height and 200 m in width.

In the French Alps, Rabatel et al. (2008) and Ravanel et al. (2012) have monitored two granitic rock walls in high mountain from survey stations located about 100 m from the rock face. According to the uncertainties, they used a thickness threshold of 0.1 m. Two rockfalls were detected in a period of 12 months in a wall of 200 m in height and 300 m in width, and 6 rockfalls in a period of 24 months in a wall of 50 m in height and 400 m in width.

It appears at first sight from this review that the spatial-temporal rockfall frequency (number of rockfalls per unit of surface and time) for a given minimal volume strongly depends on the geological and geomorphological contexts (lithology and structure of the cliff, erosion factors). The development of TLS allows to precise the frequencies corresponding to different contexts and further to determine the influence of the geological and geomorphological factors on the spatial-temporal frequency. In this paper, we study the rockfall frequency in a typical limestone cliff of the Subalpine Chains.

The cliff surveyed sit on top of a densely forested talus slope. It ensues that the survey station had to be located relatively far from the cliff, which makes the detection of rockfalls more difficult than in the previous studies.

2 Description of the cliff and measurements

The Mont Saint-Eynard (1308 m) is located 4 km to the North of the Grenoble centre and towers above a residential area of the town (Fig. 1 and 2). Its geological context has been described by Gidon (2013). The South-East face consists of, from top to bottom: a 120 m high limestone cliff (Tithonian and upper Kimmeridgian stages); a 100 m high forested slope of marl and marly limestone (Kimmeridgian stage); a 240 m high limestone cliff (Sequanian stage); a 300 m high forested talus slope, covering marl and marly limestone of the Oxfordian stage. This paper describes the results obtained for the Sequanian cliff.

The survey station was located at the foot of the talus slope, on a protection embankment at an elevation of 580 m. The inclined distance to the cliffs ranges between 625 m and 900 m. Note that no place was found closer to the cliffs. Photographs and laser measurements were carried out on August 27, 2009 and November 19, 2012.

The laser scanner technology also called LiDAR (Light Detection And Ranging), is based on the acquisition of a point cloud using a time-of-flight distance measurement of an infrared laser pulse which reflects on the topography. The raw data consist of the x, y, z coordinates of each reflection point and the intensity of the reflected pulse. The y axis corresponds to the outward axis of the laser camera and x and z axes are parallel to the sides of the scene (x is roughly horizontal).

We have used two Optech systems: ILRIS-3D in 2009 and ILRIS-LR in 2012. The main characteristics of these systems are given in Table 1. It can be seen that ILRIS-LR has a higher repetition rate, allowing a greater number of points to be measured for a given period of time. In the distance range concerned, it can also measure surfaces having a lower reflectivity than ILRIS-3D. According to the distances given above and the accuracy given in Table 1, the expected accuracy of our distance measurements ranges from about 5 cm for the closest points to 7,5 cm for the farthest ones. Two scans were taken to cover a cliff width of about 750 m.

3 Data analysis

The software 3DReshaper Application have been used to process the point clouds.

3.1 Cleaning the raw point cloud

Vegetation has a lower reflectivity than the rock making up the cliff. Thus, a reflectance threshold has been chosen to remove most of the points corresponding to vegetation. After cleaning, the point clouds consisted of 2.7 Mpt in 2009 and 12.8 Mpt in 2012. They are shown in Fig. 3. The average distance between the points ranged from 21 to 29 cm (according to the distance from the camera to the cliff) in 2009 and from 10 to 13 cm in 2012.

3.2 Georeferencing

Georeferencing the LiDAR point clouds was made by registering these with a Digital Elevation Model (1 m x 1 m) using Lambert 2 extended (x,y) coordinates and NGF IGN 69 leveling (z). The DEM is shown in Fig. 4. Then the coordinate system has been rotated in order to easily determine the width and the thickness of the fallen compartments. The width is defined horizontally, parallel to the cliff (new x direction), the thickness is defined horizontally, perpendicular to the cliff direction (new y direction) and the height is parallel to the z axis (unchanged). The positive direction is inside the cliff for the y axis and towards the East side for the x axis.

3.3 Meshing the 2012 point clouds

The more recent point cloud (2012) has been transformed in a mesh (polyhedrons), made up of 2.7 million of triangles and 1.3 million of vertex (Fig. 5a and 5b). The average distance between the vertex of the polyhedrons ranges from 26 to 36 cm (according to the distance from the camera to the cliff). Note that the number of vertex is about ten times less than the initial number of points of the cloud. This reduction is associated to the noise reduction process we used in 3DReshaper and is also necessary for numerical reasons. The registration of the 2012 point cloud with the corresponding mesh gives information about the roughness of the rock surface at the scale of the triangles making up the mesh. It appears that about 50 % of the points are closer than 1 cm from the mesh, 90 % are closer than 3 cm and 99 % are closer than 7 cm. Note that, in the later case, most of the deviations larger than 7 cm are located on vegetation areas, which have not been suppressed in the cleaning process.

3.4 Registration of the point clouds

As georeferencing with the DEM was not precise enough, the 2012 mesh and the point cloud acquired in 2009 have been registered (fitted) together in order to put them exactly in the same coordinate system. Ideally, the deviations between these objects should be due only to rockfalls occurred between 2009 and 2012. But in reality, there are other causes of deviations: (a) measurement inaccuracy; (b) the 2009 measurement points do not correspond to the 2012 ones and consequently, are not exactly on the triangles defined by the 2012 vertex (due to the curvature and the roughness of the rock surface); (c) the later cause is accentuated in areas where the triangles are large (this situation occurs particularly near the limits of the mesh); (d) vegetation element which has not been removed; (e) earth slide due to the impact of an overlying rockfall. Consequently, a deviation threshold has to be set for the detection of true rockfalls.

3.5 Detection of the rockfalls with visual checking

In a first stage, a deviation threshold was set to 0.2 m in order to make possible checking the rockfalls by comparing photographs taken in 2009 and 2012 (for a lower threshold, most of the rockfalls are not visible on photographs). A rockfall has been considered certain when a positive deviation is observed and the comparison of the 2009 and 2012 photos shows that a rockfall has occurred between these dates. Such a comparison is shown in Fig. 6. When a positive deviation is observed and the comparison of the 2009 and 2012 photos shows that no rockfall has occurred, the deviation has been considered to be a false rockfall. The false rockfalls which have been obtained are due to the conditions (c) or (d) expressed in the later paragraph. When a positive deviation is observed and the photo comparison cannot conclude if a rockfall has occurred or not, the deviation has been considered to be an uncertain rockfall if the conditions (c) or (d) occur or a probable rockfall if these conditions don't occur. This situation occurs more and more when the extent of the deviation zone decreases (Fig. 7). The reason is that small rockfalls are difficult to observe on photographs. Fig. 7 shows the proportions of certain, probable, uncertain and false rockfalls as a function of the rockfall volume.

For the 162 certain and probable rockfalls detected, the volume has been calculated by creating a watertight mesh, starting from the 2009 and 2012 surfaces of the fallen rock compartment, which were not initially attached. This procedure is manual and time consuming. At this stage of analysis, 169 events have been detected, out of which 2 false rockfalls and 5 uncertain ones.

The minimal and maximal volumes detected are respectively of 0.018 m^3 and 81 m^3. The complementary cumulative distribution function of the rockfall volume is shown in Fig. 8. A power law has been fitted to the data. It can be seen that the fitting is better when considering only the volumes greater than 0.1 m^3.

3.6 Detection of the rockfalls without visual checking

In a second stage, the deviation threshold has been lowered in order to detect smaller rockfalls, which cannot be checked with photographs. According to the accuracy expected (Sect. 2), the deviation threshold has been set to 0.1 m. In this stage, 295 additional events have been detected, out of which 229 probable rockfalls. Although smaller volumes are detected with a deviation threshold of 0.1 m, it occurs that the minimal volume detected is the same (0.018 m^3) as with the 0.2 m threshold. The complementary cumulative distribution function of the rockfall volume is shown in Fig. 9. The fitting to a power law is better when considering only the volumes greater than 0.05 m^3.

4 Discussion

The distribution function of the rockfall volume has been studied by several authors (see reviews in Dussauge-Peisser et al., 2002, and Brunetti et al., 2009). Most of them found that the complementary cumulative distribution function is well fitted by a power law:

$$N = aV^{-b} \quad (1)$$

where V is the rockfall volume, N is the number of rockfalls larger than V, a and b are constants. The validity of a power law to describe the rockfall volume distribution has been tested by Dussauge-Peisser et al. (2003) using a χ^2 test. The constant a represents the number of rockfalls whose volume is greater than 1 m^3 (assuming the law is valid for this volume range). It depends on the size of the cliff, the length of the observation period and the geological and geomorphological context. On the contrary, the exponent b only depends on the geological and geomorphological context. Its value has been determined for some different contexts (Dussauge-Peisser et al., 2002). For the particular contexts studied up to now, it ranges from 0.4 to 0.72. Its standard deviation has been estimated in some cases (Dussauge-Peisser et al., 2003) using a maximum likelyhood method:

$$\sigma = b / \sqrt{N}_0 \quad (2)$$

where N_0 is the number of events considered and b is the exponent value in Eq. (1).

Fig. 8 shows the volume distribution function for the rockfalls detected in this study using a threshold of 0.2 m, most of which having been checked visually (Fig. 7). It can be seen that the distribution function is well fitted by a power law for volumes greater than 0.2 m^3, with an exponent of 0.69 ± 0.07 and a correlation coefficient of 0,983. But the volumes lower than 0.2 m^3 are underrepresented, probably by under-sampling. This is confirmed by Fig. 9, which shows the volume distribution function for a threshold of 0.1 m. This function is well fitted by a power law for volumes greater than 0.05 m^3, with an exponent of 0.75 ± 0.04 and a correlation coefficient of 0,994. Now the volumes lower than 0.05 m^3 are underrepresented. This underrepresentation can be due to the limited resolution of the investigation method or reflects the real distribution of the rockfall volume. The fact that the exponent value is not significantly changed by passing from the visually checked rockfalls (Fig. 7) to the numerically detected ones (Fig. 8), suggests that the obtained inventory is exhaustive for volumes greater than 0.05 m^3.

For comparing the rockfall activities of cliffs in different geological and geomorphological contexts, it is necessary to consider the number of rockfalls per unit of time and space (spatial-temporal frequency). For this purpose, we introduce the rockfall activity parameter A_{st}, which is a (from Eq. 1) divided by the cliff surface and the length of the observation period. In order to calculate this parameter for the Mont Saint-Eynard lower cliff (Sequanian), a mean height of 200 m and a width of 750 m have been considered, which give a value of 0.85 rockfalls per year and per hm^2, using the a-value of 41 given in Fig. 8.

Hantz et al. (2003) analyzed the cumulative distribution of rockfall volumes between 10^2 and 10^7 m^3, occurred in the 120 km long limestone cliffs of the Grenoble area, which include the Mont Saint-Eynard cliff. They found that a power law well describes the distribution, with an exponent of 0.55 ± 0.11 and a rockfall activity of 0.0047 rockfalls per year and per hm^2. It appears that both parameters b and A_{st} are significantly different for the two considered rock fall populations: b = 0.75 ± 0.04 and A_{st} = 0.85 for the Mont Saint-Eynard; b = 0.55 ± 0.11 and A_{st} = 0.0047 for the Grenoble area. As the power law parameters for the two inventories were determined from volumes ranging respectively from 0.05 m^3 to 100 m^3 and from 100 m^3 to 10^7 m^3, it is more pertinent to compare the rockfall activities by using the numbers of rockfalls larger than 100 m^3, which occur per century and per hm^2. These numbers are respectively of

2.7 and 0.037, giving a ratio of 72. Several reasons can be proposed to explain this strong discrepancy:

(a) The rockfalls for the Grenoble area were known from a historical inventory which is probably not exhaustive.

(b) Most of the rockfall volumes for the Grenoble area were estimated from historical sources, with more uncertainty than for the Mont Saint-Eynard.

(c) The cliffs of the Grenoble area consist of different calcareous rocks of Jurassic and Cretaceous age, including mostly massive limestones (metric to decametric thickness), whereas the cliff studied consists only of thinly bedded limestone of Sequanian stage (thickness of 20-50 cm).

5 Conclusions

Terrestrial laser scanner can be used to detect rockfalls which occur in high rock walls from a survey station located up to 900 m from the cliff. Using a threshold of 0.1 m in term of distance variation, 344 rockfalls larger than 0.05 m^3 have been detected for a period of 1180 days, in a rock wall of width 750 m and height 200 m.

The complementary cumulative distribution of the rockfall volume is well fitted by a power law, with an exponent b of 0.75 ± 0.04 and a rockfall activity parameter A_{st} of 0.85 rockfalls per year and per hm^2. These parameters characterize the rockfall frequency in a thinly bedded limestone cliff of the Subalpine Chains.

They are significantly different from those which have been obtained from a historical rockfall inventory covering 120 km of cliff consisting mostly of massive limestone: For this inventory, the b-value is 0.55 ± 0.11 and the theoretical number of rockfalls larger than 100 m^3, which occur per century and per hm^2, is 0.037 instead of 2.7 for the thinly bedded limestone. Terrestrial laser scanning of large cliff surfaces of massive limestone in the Subalpine Chains is needed to better investigate the rockfall frequency in these cliffs.

Acknowledgements

The authors thank the Région Rhône-Alpes and the VOR Research Network for their funding. They also thank Alex Loye, Benoît Fragnol, Battista Matasci and Jérémie Voumard who performed laser scannings.

References

Abellan, A., Calvet, J., Vilaplana, J.M., Blanchard, J.: Detection and spatial prediction of rockfalls by means of terrestrial laser scanner monitoring, Geomorphology, 119, 162-171, 2010.

Abellan, A., Vilaplana, J.M., Calvet, J., Garcia-Selles, D., Asensio, E. : Rockfall monitoring by terrestrial laser scanning – case study of the basaltic rock face at Castellfollit de la Roca (Catalonia, Spain), Nat. Hazards Earth Syst. Sci., 11, 829-841, 2011.

Brunetti, M.T., Guzzetti, F., Rossi, M.: Probability distributions of landslide volumes, Nonlin. Processes Geophys., 16, 179-188, 2009.

Dewez, T.J.B., Rohmer, J., Regard, V., Cnudde, C. : Probabilistic coastal cliff collapse hazard from repeated terrestrial laser surveys : case study from Mesnil Val (Normandy, northern France), Journal of Coastal Research, 65, 702-707, 2013.

Dussauge-Peisser, C., Helmstetter, A., Grasso, J-R., Hantz, D., Jeannin, M., Giraud, A.: Probabilistic approach to rock fall hazard assessment: potential of historical data analysis. Nat. Hazards Earth Syst. Sci., 2, 15-26, 2002.

Dussauge-Peisser, C., Grasso, J.R., Helmstetter, A.: Statistical analysis of rockfall volume distribution : Implication for rockfall dynamics, J. Geophys. Res., 108, 2286, doi:10.1029/2001/JB000650, 2003.

Fell, R., Ho, K.K.S., Lacasse, S., Leroi, E.: A framework for landslide risk assessment and management. In: Landslide Risk Management, Hungr, Fell, Couture & Eberhardt (eds), Taylor & Francis Group, London, 3-25, 2005.

Gidon, M.: Le Saint-Eynard, Corenc, Meylan, http://www.geol-alp.com/chartreuse/6_sommets_ch/st_eynard.html, 2013.

Hantz, D., Vengeon, J.M., Dussauge-Peisser, C.: An historical, geomechanical and probabilistic approach to rock-fall hazard assessment, Nat. Hazards Earth Syst. Sci., 3, 693-701, 2003.

Hantz, D.: Quantitative assessment of diffuse rockfall hazard along a cliff foot, Nat. Hazards Earth Syst. Sci., 11, 1303–1309. 2011.

Hungr, O., Evans, S.G., Hazzard, J.: Magnitude and frequency of rock falls and rock slides along the main corridors of southwestern British Columbia, Can. Geotech. J., 36, 224-238, 1999.

Lim, M., Rosser, N.J., Allison, R.J., Petley, D.N.: Erosional processes in the hard rock coastal cliffs at Staithes, North Yorkshire, Geomorphology, 114, 12-21, 2010.

Picarelli, L., Oboni, F., Evans, S.G., Mostyn, G., Fell, R.: Hazard characterization and quantification. In: Landslide Risk Management, Hungr, Fell, Couture & Eberhardt (eds), Taylor & Francis Group, London, 27-61, 2005.

Rabatel, A., Deline, P., Jaillet, S., Ravanel, L.: Rock falls in high-alpine rock walls quantified by terrestrial lidar measurements: A case study in the Mont Blanc area, Geophys. Res. Lett., 35, L10502, doi:10.1029/2008GL033424, 2008.

Ravanel, L., Deline, P., Lambiel, C., Vincent, C.: Instability of a high alpine rock ridge: The lower Arête des Cosmiques, Mont Blanc massif, France, Geografiska Annaler, Series A, Physical Geography, doi:10.1111/geoa.12000, 2012.

Rosser N.J., Petley D.N., Lim M., Dunning S.A., and Allison, R.J.: Terrestrial laser scanning for monitoring the process of hard rock coastal cliff erosion, Q. J. Eng. Geol. Hydrogeol., 38, 363-375, 2005.

1 Table 1. Main characteristics of the laser scanners used.

Parameter	ILRIS-3D	ILRIS-LR
Range 80% reflectivity	1200 m	3000 m
Range 10% reflectivity	400 m	1330 m
Minimum range	3 m	3 m
Laser repetition rate	2500 to 3500 Hz	10 000 Hz
Raw range accuracy	7 mm @ 100 m	7 mm @ 100 m
Raw angular accuracy	8 mm @ 100 m	8 mm @ 100 m
Field of view	40° x 40°	40° x 40°
Minimum step size	0,001146° (20 µrad)	0,001146° (20 µrad)
Maximum density	2 cm @ 1000 m	2 cm @ 1000 m
Rotational speed	0,001 to 20°/sec	0,001 to 20°/sec
Beam diameter	22 mm @ 100 m	27 mm @ 100 m
Beam divergence	0,009740° (170 µrad)	0,014324° (250 µrad)
Laser wavelength	1535 nm	1064 nm
Integrated camera	3,1 MP	3,1 MP

2

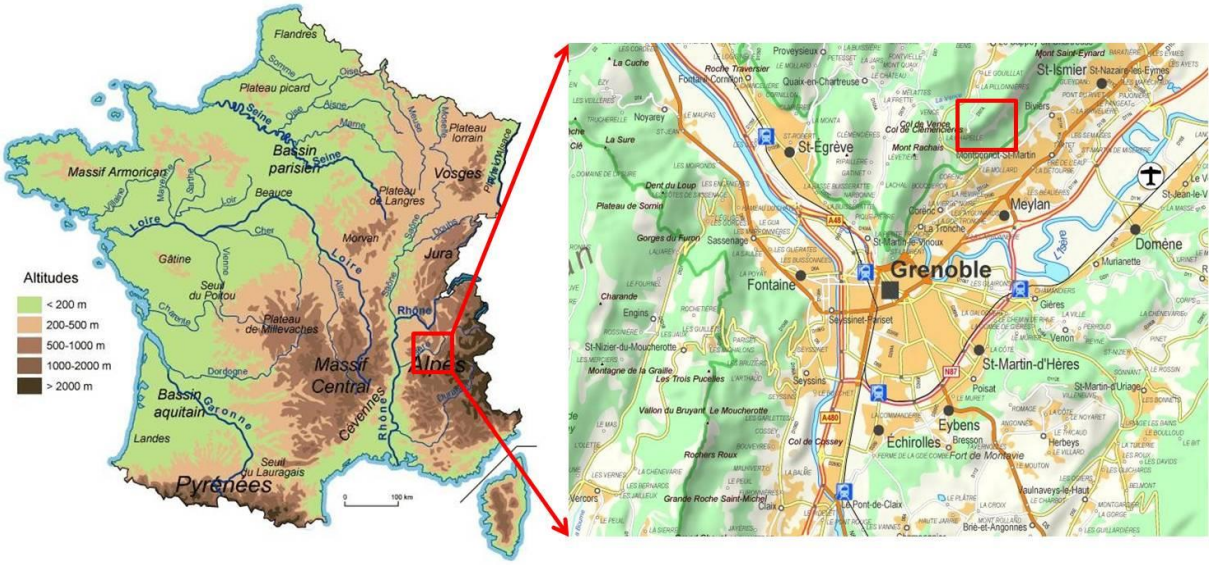

Figure 1. Location of the Mont Saint-Eynard. Inhabited areas appear in beige in the right map.

Figure 2. Photograph of the Mont Saint-Eynard cliff.

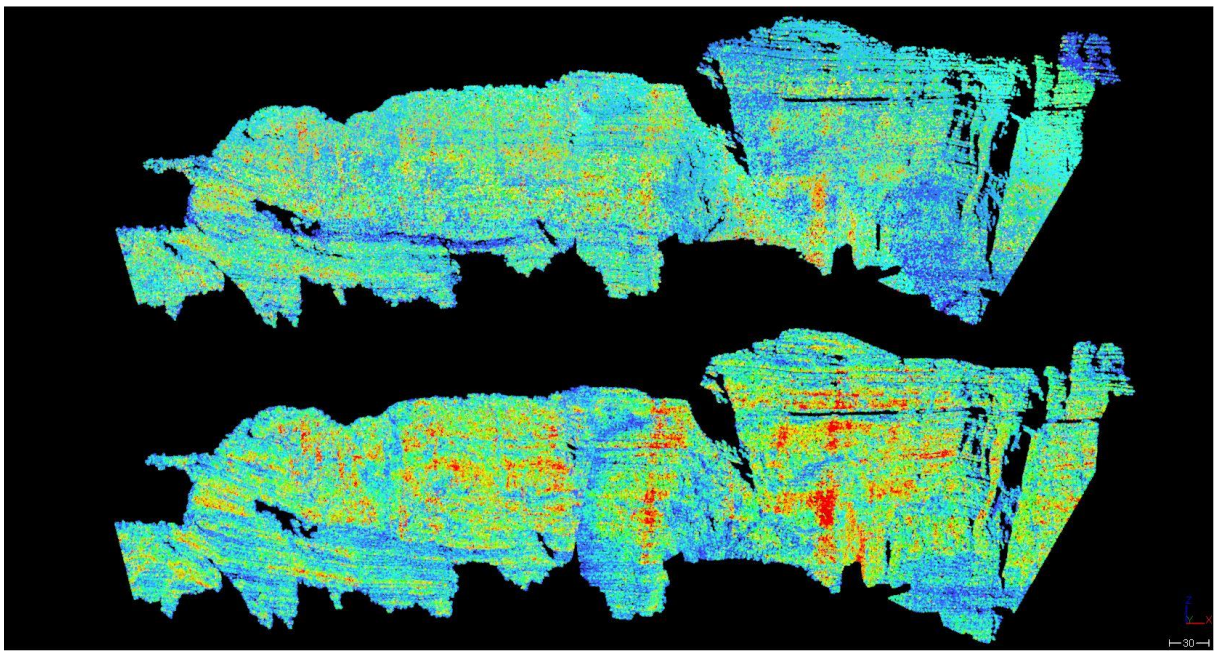

Figure 3. Point clouds measured in 2009 (high) and 2012 (low). Red: high reflectance. Blue: low reflectance.

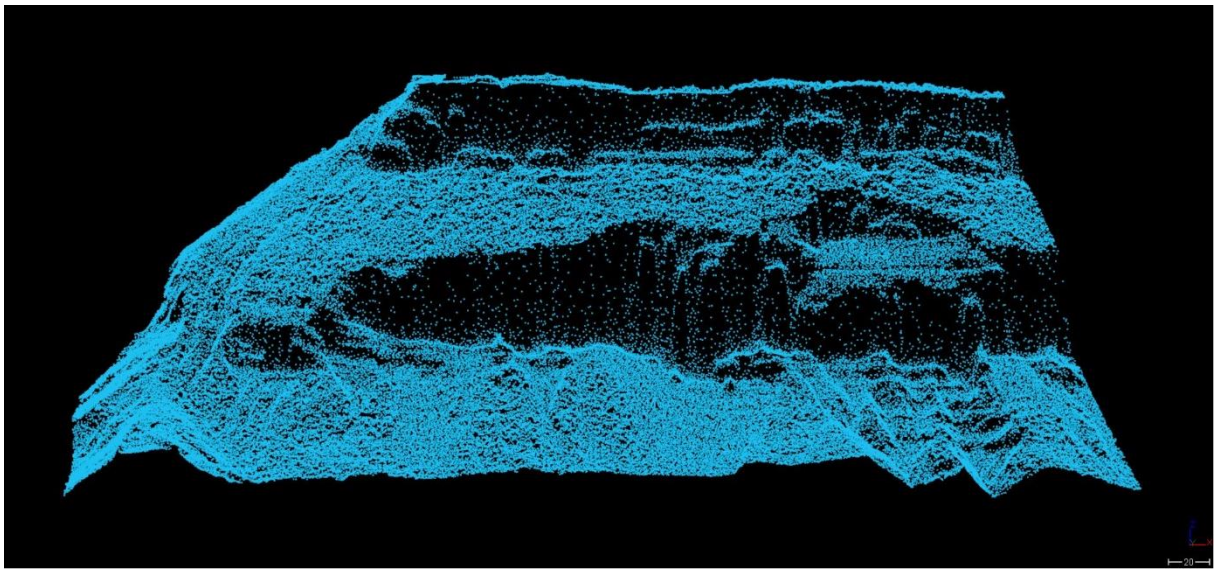

Figure 4. Digital Elevation Model used for georeferencing (1 m x 1 m grid).

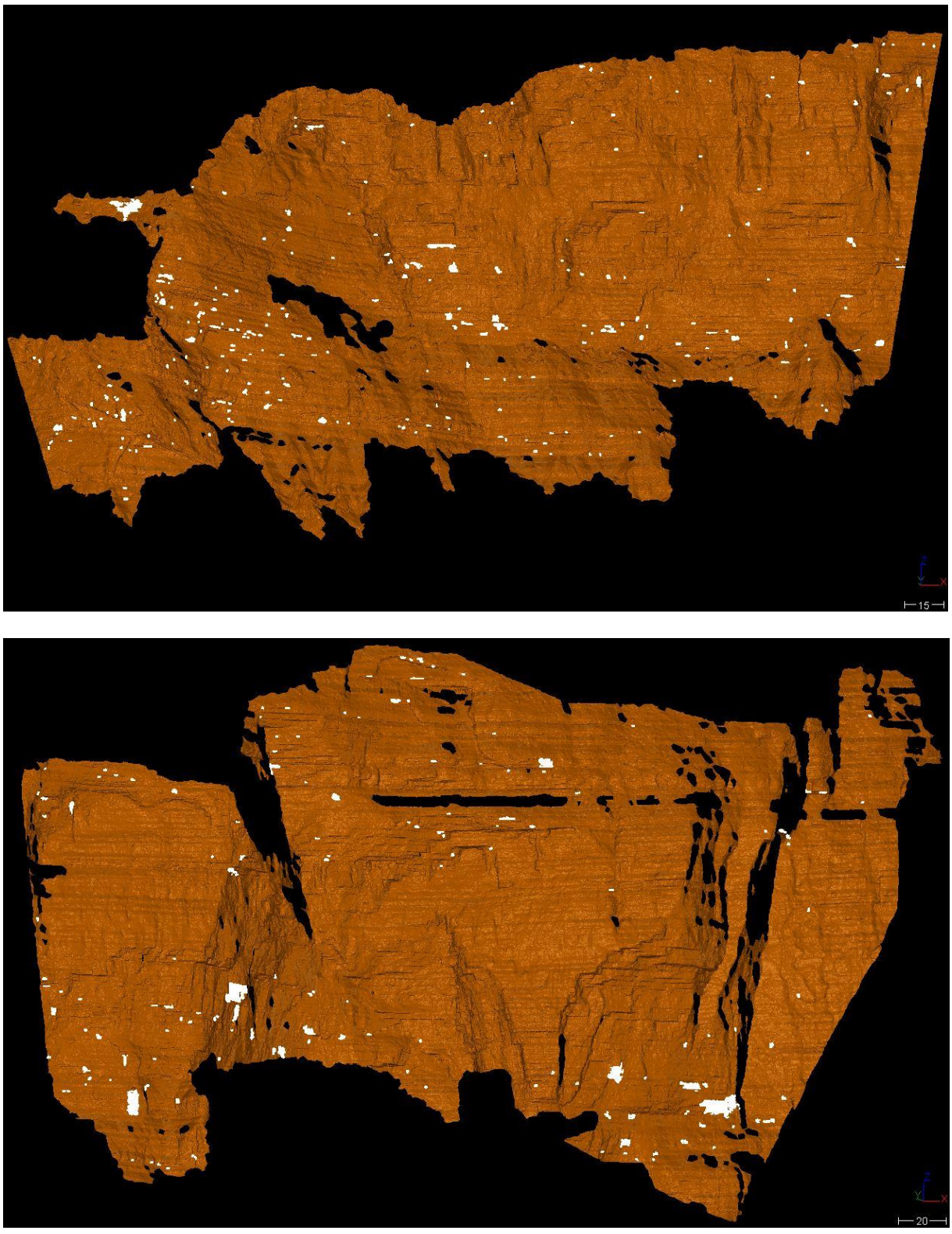

Figure 5. Upper: Mesh for the left scene 2012 and rockfall detected (white spots). Lower: Mesh for the right scene 2012 and rockfall detected (white spots).

Figure 6. Rockfall proven by comparison of 2009 and 2012 photographs (81 m^3).

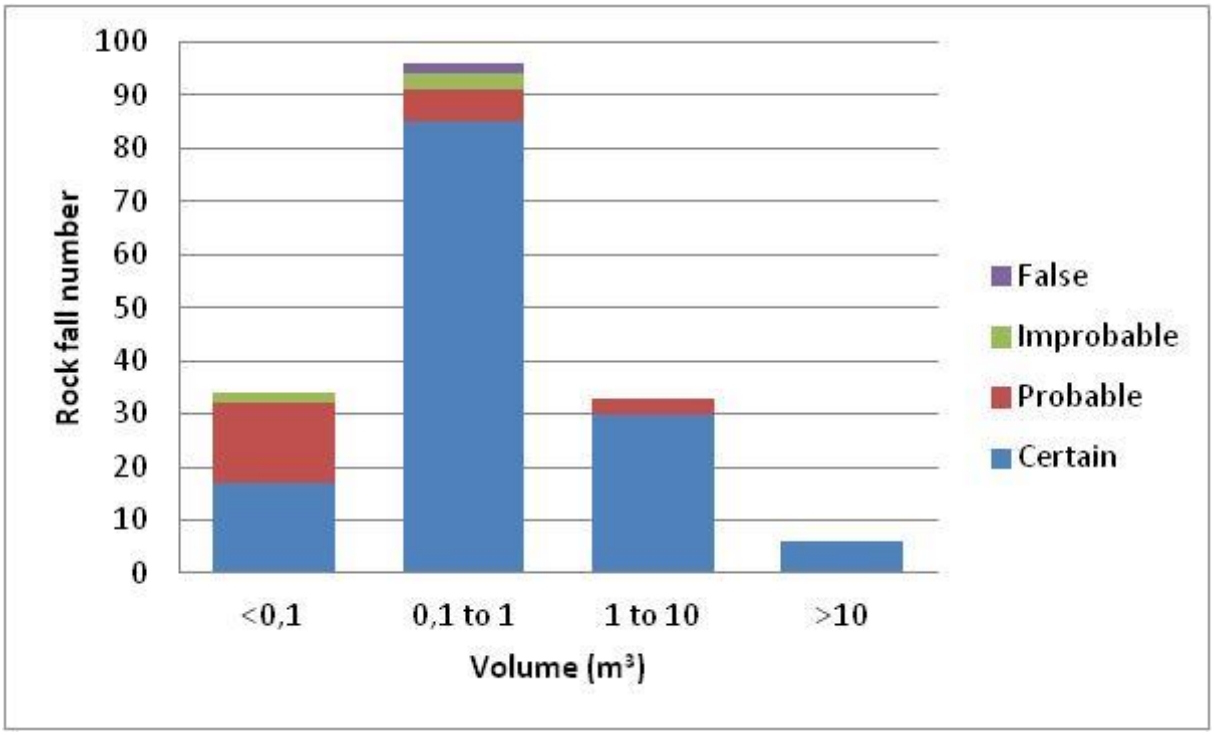

Figure 7. Proportions of certain, probable, uncertain and false rockfalls as a function of the rockfall volume, for a deviation threshold of 0.2 m.

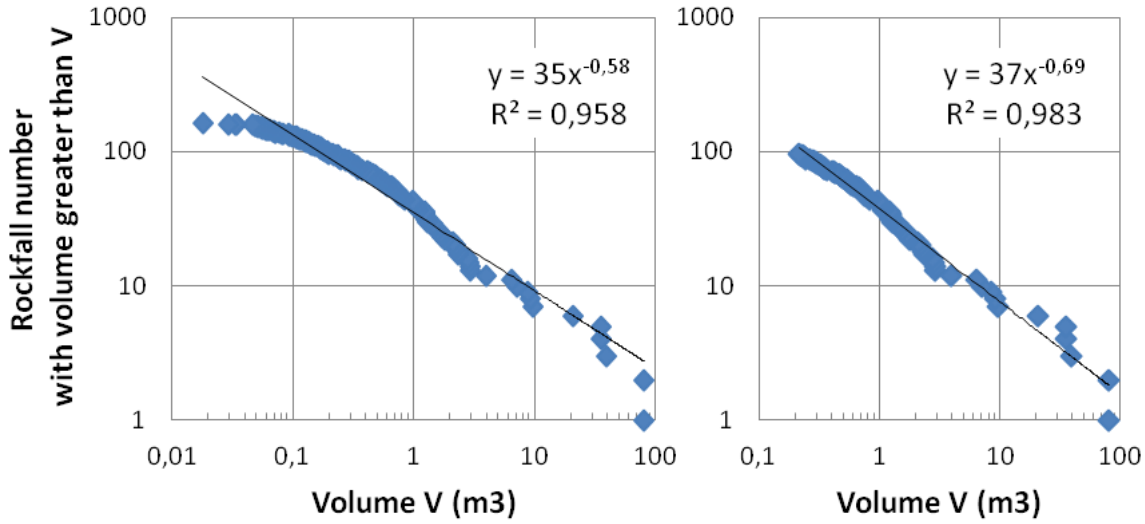

1

2

3 Figure 8. Distribution function of the rockfall volume for a deviation threshold of 0.2 m.

4 Left: Volume > 0.01 m^3 (162 events). Right: Volume > 0.2 m^3 (96 events).

5

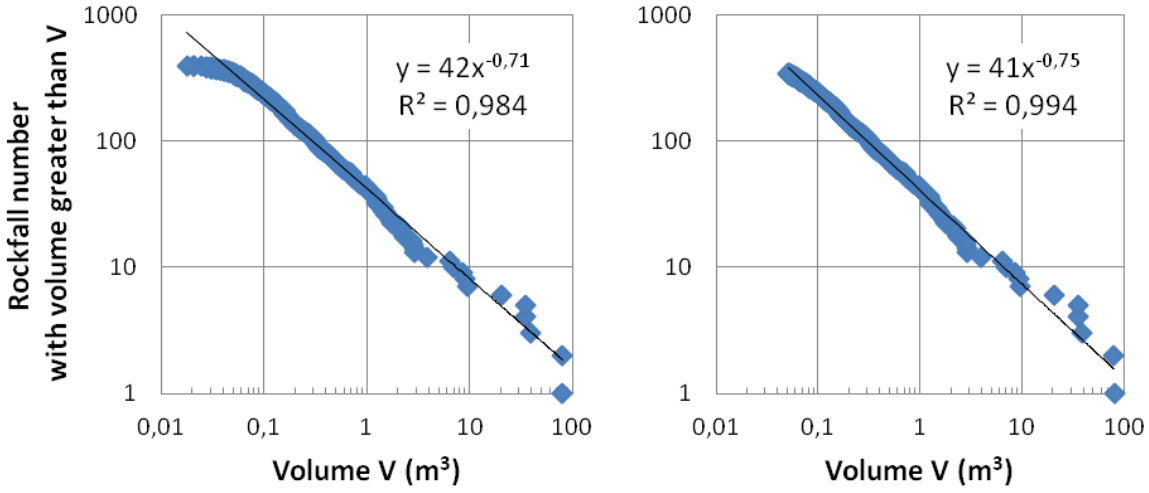

6

7

8 Figure 9. Distribution function of the rockfall volume for a deviation threshold of 0.1 m.

9 Left: Volume > 0.01 m^3 (391 events). Right: Volume > 0.05 m^3 (344 events).